Optical Probing of Rayleigh Wave Driven Magnetoacoustic Resonance

P. Kuszewski, J.-Y. Duquesne, L. Becerra, A. Lemaitre, S. Vincent, S. Majrab, F. Margaillan, C. Gourdon, L. Thevenard

Optical probing of wave driven magneto-acoustic resonance

P. Kuszewski,[1] J.-Y. Duquesne,[1] L. Becerra,[1] A. Lemaître,[2] S. Vincent,[1] S. Majrab,[1] F. Margaillan,[1] C. Gourdon,[1] and L. Thevenard[1]

[1] *Sorbonne Université, CNRS, Institut des Nanosciences de Paris, 4 place Jussieu,75252 Paris France*
[2] *Centre de Nanosciences et de Nanotechnologies, CNRS, Univ. Paris-Sud, Université Paris-Saclay, 91460 Marcoussis, France*

(Dated: August 2, 2018)

The resonant interaction of electrically excited travelling surface acoustic waves and magnetization has hitherto been probed through the acoustic component. In this work it is investigated using time-resolved magneto-optical detection of magnetization dynamics. To that end, we develop an experimental scheme where laser pulses are used both to generate the acoustic wave frequency and to probe magnetization dynamics thus ensuring perfect phase locking. The light polarization dependence of the signal enables to disentangle elasto-optic and magneto-optic contributions and to obtain the in-plane and out-of-plane dynamic magnetization components. Magnetization precession is proven to be driven solely by the acoustic wave. Its amplitude is shown to resonate at the same field at which we detect piezo-electrically the resonant attenuation of the acoustic wave, clearly evidencing the magneto-acoustic resonance with high sensitivity.

I. INTRODUCTION

Recent years have witnessed a renewed and growing interest in the use of acoustic waves to excite spin waves as an alternative, fast, efficient, and heat-free means to generate and control (possibly coherently and remotely) information in magnetic materials[1–16]. Magnetization switching[3,7,11,12,16], and parametric excitation of spin waves[9,13] have for instance been demonstrated, thus opening new opportunities for applications. The efficiency of acoustic waves relies on magneto-elastic coupling that occurs in magnetostrictive materials. Electrically excited surface acoustic waves (SAWs), with typical frequencies up to the GHz range are particularly well suited to excite magnetization dynamics in ferromagnetic magnetostrictive layers. Their interaction was evidenced using piezo-electric detection of SAW-induced ferromagnetic resonance (SAW-FMR)[1,4]: the SAW amplitude and velocity resonantly decrease when the spin wave frequency is varied across the SAW frequency by an applied magnetic field. However, spin waves have not been concomitantly observed. Time-resolved detection of magneto-optical effects using probe laser pulses indeed could provide a direct and very sensitive method to access magnetization dynamics[17]. This requires a non-trivial synchronization of the electrical SAW generation with probe laser pulses. Until now this difficulty has been bypassed by utilizing fairly cumbersome synchrotron X-ray radiation[18].However no resonant magnetization dynamics have been observed .

In this article, we demonstrate optically the forced magnetic precession induced by travelling SAWs. To that end, we implement a table-top set-up to generate SAW bursts electrically using interdigitated transducers (IDTs) with perfect phase locking to laser pulses, which enables the optical investigation of time- and space-resolved magnetization dynamics excited by the SAW. We illustrate the potentiality of this technique using a ferromagnetic semiconductor layer of GaMnAs on piezoelectric GaAs, taking advantage of its low FMR frequency which is easily tunable across the SAW frequency, and its sizable magneto-optical effects. Using the probe light polarization and the magnetic field dependencies of the time-resolved signal we separate the magneto-optical from the pure elasto-optical contribution. The in-plane and out-of plane magnetization dynamical components display the dependencies on the magnetic field expected from the SAW-induced torque acting on the magnetization[19,20]. Finally, we show that resonant magnetic excitation appears concomitantly with resonant SAW absorption, the detection of the former being more sensitive than the latter.

II. EXPERIMENTAL SETUP

SAWs such as Rayleigh waves are easy to implement and thus find applications in various fields of soft and condensed matter physics[21–24]. With frequencies up to the GHz, their dynamical strain components are confined within a few µm from the surface, and can thus efficiently interact with a magnetic layer on a substrate. SAWs can be generated either optically via thermoelasticity[5,10,13,25] or electrically via the piezoelectric effect using IDTs[26,29]. The simplest IDT consists of two comb-shaped electrodes in zipper configuration that work as capacitors on a piezoelectric surface. When a radio-frequency (RF) voltage at f_{SAW} is applied, SAWs are generated and propagate on either side of the IDT. The wavelength λ_{SAW} of the excited SAW is determined by the period of the electrode teeth. Frequency and wavelength are related by $\lambda_{SAW} = \frac{v_R}{f_{SAW}}$ where v_R is the Rayleigh velocity. Typical λ_{SAW} values are around a few microns. The strain components excited with the IDT are: longitudinal ε_{xx} ($x \parallel \mathbf{k}_{SAW}$), transverse ε_{zz} (z perpendicular to

the surface) and shear ε_{xz} (negligibly small close to the surface)[26]. In more sophisticated IDT architectures it is possible to excite overtone harmonics of the fundamental frequency, such as the split-52 design[27], which is used in this work. Optical time-resolved measurement of magnetization dynamics requires a fixed phase between the laser pulses and the acoustic bursts. The most common solution is a phase-locked loop[28]. The 'master' clock imposes the repetition rate of the 'slave' laser. The laser cavity length is continuously adjusted in order to meet the set frequency. We propose a simpler, elegant, and low-cost alternative approach where f_{SAW} is built from the laser repetition rate thereby ensuring a stable phase lock. Two research groups have very recently reported independently similar synchronization methods[18,29].

In order to generate the SAW RF frequency, a small fraction of a Ti:Sapphire laser at ∼75 MHz repetition rate (f_L) was directed to a Silicon photodiode (Thorlabs PDA10A-EC, bandwidth 150 MHz) to pick up the laser fundamental frequency (Fig. 1(a)). Using different RF multipliers, multiples of the laser frequency were then generated: $n\,f_L$, where n = 2, 4, 6, 8. To ensure that $n\,f_L$ is free of any harmonics, the signal was filtered with 50 dB rejection band pass filters. The signal level was adjusted with a linear 40 dB amplifier and a set of attenuators.

The larger fraction of the 130 fs laser pulses (wavelength 722 nm) was sent to a pulse selector (Fig. 1(a)). The repetition rate was reduced by a factor 300 to f_{rep} = 250 kHz. This beam was used to probe the magnetization and strain dynamics in a time window of 12 ns controlled with a motorized optical delay line stage.

As we shall see hereafter the IDT needs to be fed with a pulsed RF signal. In order to fabricate these pulses the $n\,f_L$ CW RF signal was mixed with a 400 ns-wide rectangular pulse train from a pulse generator (Keysight 81150A) at the pulse picker frequency f_{rep} thus ensuring that both the envelope frequency and the RF frequency of the SAW are commensurate with f_L. With the pulse generator we could modify the burst duration and its arrival time (electronic delay) to the transducer. The 'edge-to-reference' jitter[30] defined as the timing variation between the rising edge of the rectangular pulse and the optical pulse shows a standard deviation σ = 13.1 ps comfortably below 1% of the highest SAW period.

The linearly polarized laser pulses at f_{rep} were focused on the sample surface with a long working distance objective lens with numerical aperture 0.4. The laser beam reflected off the sample traveled through the same objective. The polarization rotation induced by the dynamical magnetization and strain components was detected by a balanced optical bridge relying on magneto-optical effects[17,31] and the photo-elastic (PE) effect[26], respectively. The bridge output was demodulated by a lock-in amplifier at the frequency of a mechanical chopper f_{ch}=541 Hz inserted on the laser beam before the slow photodiode (Fig. 1(a)), *i.e.* modulating the excitation SAW. Polarization rotations as small as 0.1 µrad can routinely be measured.

The sample was a 45 nm thick, in-plane magnetized $Ga_{0.95}Mn_{0.05}As$ layer on a (001) GaAs substrate, annealed for 16 h at 200^{o}C, with a Curie temperature T_C = 120 K. It was placed in an Oxford MicroStat HiRes cryostat that ensures the required mechanical stability and optical access. The GaMnAs layer has a strong uniaxial magnetic anisotropy with the easy axis along [1-10] and exhibits a large magneto-elastic coupling[16]. An in-plane magnetic field aligned with the hard axis [110] was applied to decrease the precession frequency and make it cross the SAW frequency. A 2x2 mm^2 square mesa of GaMnAs was prepared by chemical etching. At two opposite ends a set of 42 nm thick Aluminum IDTs with 1 mm aperture were deposited on the GaAs (Fig. 1(a)). In order to provide efficient operation of the IDTs even when varying the temperature (given the temperature dependence of $v_R(T)$) and to achieve a compromise between excitation efficiency and bandwidth, the IDTs were designed as 25 pairs of split-52 electrodes. With a digit width and inter-digit spacing of 1.9 µm, the fundamental period was λ_{SAW}=19 µm. This ensured that the wavelength of all excited SAW frequencies was substantially larger than the laser spot diameter (full-width at half maximum of about 1 µm). The RF voltage applied to the IDT triggers the propagation of a SAW along the [1-10] axis. The RF power was set to 25 dBm for most data presented here. We used the second IDT to detect the SAW electrically by the inverse piezoelectric effect after it had travelled d = 2.03 mm along the layer surface. Figure 2 presents an oscilloscope trace of the recorded signal (red line). The first 400 ns burst is the electromagnetic radiation. It travels with the speed of light and appears immediately at the receiver. After around $t_{trans} = \frac{d}{v_R}$ = 730 ns the acoustic echo arrives (v_R ≈2780 m s^{-1}). The pulsed RF allows to separate in time the electromagnetic radiation and the acoustic echo. The risetime of the acoustic echo is defined by the IDT geometry, the SAW velocity, and the burst duration[26].

III. RESULTS AND DISCUSSION

Figure 1(b) shows the time-resolved polarization rotation (TRPR) at 60 K for excitation SAW frequencies 151, 301, 452 and 602 MHz as a function of the optical delay. The frequency of the detected signals matches exactly the excitation frequency. The amplitude of the signal varies with the magnetic field up to T_C, above which we observe only a field independent signal. This proves that the TRPR signal contains both a magnetic (field-dependent) contribution and a non-magnetic one arising from the elasto-optic effect.

In order to prove that the optically detected dynamics is indeed triggered by the SAW we monitored the amplitude of the TRPR signal at various delays after the beginning of the the RF burst by setting an electronic delay $\Delta\tau$ between the electric excitation and the optical

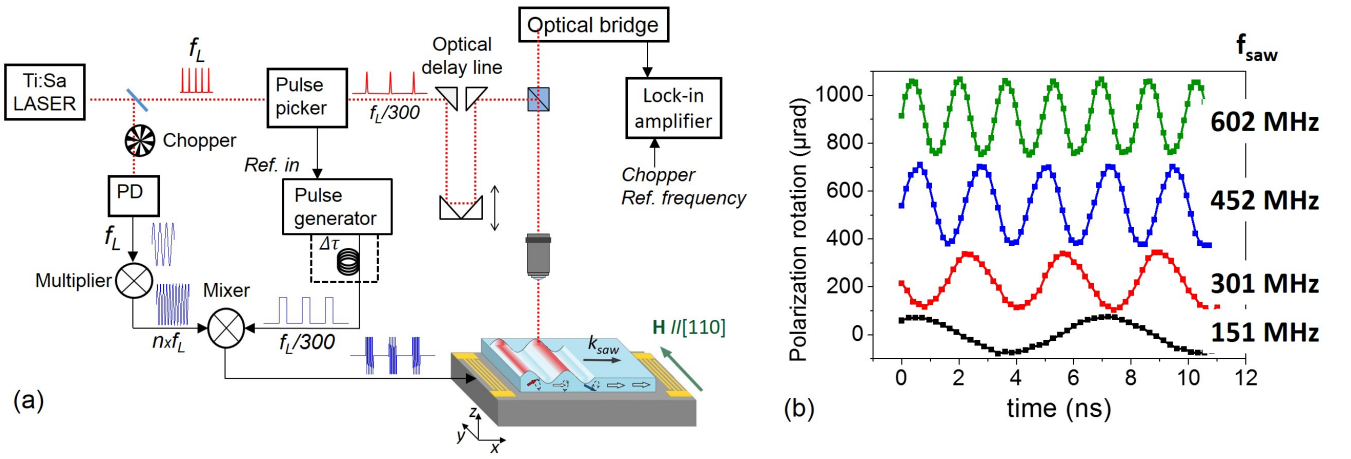

FIG. 1. (a) Schematics of the experimental set-up, (b) Time-resolved polarization rotation signal for four SAW frequencies (vertically off-set for clarity). The probe polarization was set at 60° with respect to $\mathbf{k}_{SAW}$. The applied magnetic field was 19.5 mT. The temperature was T=60K.

pulse probe (Fig. 1(a)). First the probe beam was set at 100 µm from the receiving IDT (1.9 mm from the emitter, open circle in the sample scheme of Fig. 2). The open circle symbol curve represents the amplitude of the TRPR oscillations versus the electronic delay. It has the same shape as the acoustic echo and peaks slightly before the arrival of this echo on the receiving IDT, in agreement with the location of the detection spot. Then the probe beam was positioned 67 µm from the emitter IDT (full circle in the sample scheme of Fig. 2). The full circle curve represents the amplitude of the oscillations versus the electronic delay. It also has the same shape as the acoustic echo and is detected earlier, in agreement with the position of the detection spot. The 20% burst amplitude decrease from one burst to the other can be directly correlated to the loss of acoustic amplitude via magneto-elastic interaction, as will be seen further (Fig. 4(g)). For both spot positions, no signal is observed at the arrival time of the electromagnetic radiation. These results show that the TRPR signal is indeed generated by the SAW.

In order to disentangle the magneto-optic and the elasto-optic contributions in the TRPR signal we analyze the dependence of the signal on the probe light polarization and the applied magnetic field. The elasto-optic effect gives rise to a dynamic birefringence with axes parallel and perpendicular to the SAW wavevector $\boldsymbol{k}_{SAW}$. The resulting rotation of linear polarization is proportional to the P_{44} component of the elasto-optic tensor of the cubic GaAs and the ε_{xx} strain component[32–34]. It does not depend on the magnetic field. Besides we expect the contribution from two magneto-optical effects[17,31] : the polar magneto-optical Kerr effect (PMOKE) sensitive to the out-of-plane dynamic component of the magnetization $\delta\theta$ and independent of the incoming polarization and the (weaker) Voigt effect (magnetic linear dichroism (MLD)) sensitive to the in-plane dynamic component of

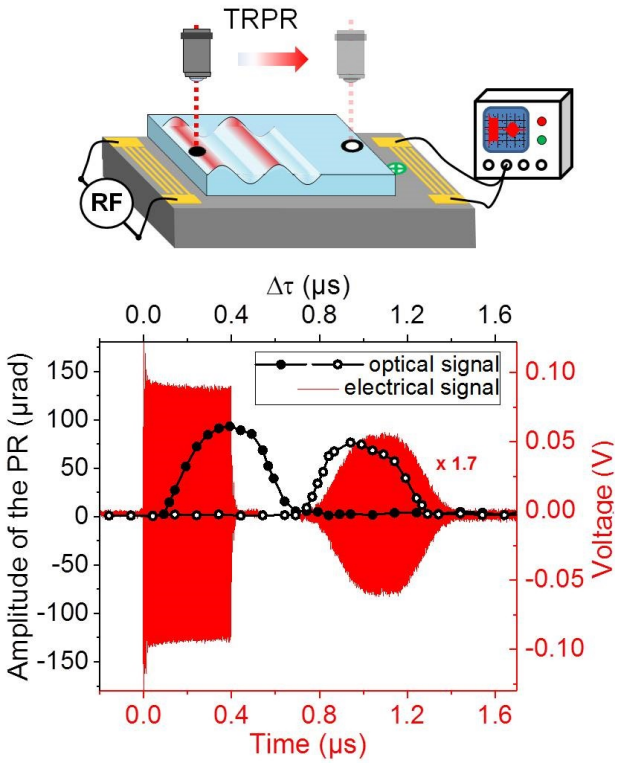

FIG. 2. Time-domain signal detected electrically (red solid line) by an oscilloscope, and amplitude of the optically detected TRPR oscillations (circles) as a function of the electronic delay. TRPR was measured in two places on the sample (open and closed symbols on the scheme). The crossed-circle symbol indicates where the optical SAW-FMR data shown in Fig. 4(h) was taken. The surface amplitudes of the excited SAW strain components are $\varepsilon_{xx} = 4.8 \times 10^{-5}$ and $\varepsilon_{zz} = 2.2 \times 10^{-5}$ estimated following the procedure described in ref.[16]. The SAW frequency is 452 MHz, the applied field is $\mu_0 H$ =20 mT, the polarization angle is β=30 deg.

the magnetization $\delta\phi$ and to the field-dependent in-plane equilibrium orientation of the magnetization $\phi_0(H)$. The TRPR signal can therefore be expressed as[17,26,31]:

$$\begin{aligned}\delta\beta &= K\delta\theta(H,t) + 2V\delta\phi(H,t)\,\cos\left(2\left(\beta-\phi_0(H)\right)\right) \\ &\quad + P_E\varepsilon_{xx}(t)\,\sin 2\beta \qquad (1)\\ &= K\delta\theta(H,t) + 2V\delta\phi(H,t)\cos 2\phi_0(H)\,\cos 2\beta \\ &\quad + \left(2V\delta\phi(H,t)\,\sin 2\phi_0(H) + P_E\varepsilon_{xx}(t)\right)\sin 2\beta \qquad (2)\end{aligned}$$

where β is the angle of the probe polarization with respect to $\boldsymbol{k}_{SAW}$, K and V are the Kerr and Voigt magneto-optical coefficients, respectively, and $P_E = Re\left(n^3P_{44}/(n^2-1)\right)$ is the elasto-optic coefficient with n the refractive index. Indeed the experimental TRPR signal shows a clear dependence on the probe polarization (Fig. 3(a)) and on the magnetic field (Fig. 3(b)). For each time and field value, the signal is fitted as a function of β by $\delta\beta = F_\theta + G_\phi\cos 2\beta + H_{\phi\varepsilon}\sin 2\beta$. The resulting fit is very good as seen in Fig. 3(b). The offset that appears under the application of a magnetic field $\mu_0 H$ =6 mT is related to the PMOKE signal $F_\theta = K\delta\theta$. The change of the phase is a good indication of the presence of MLD. The resulting F_θ, G_ϕ, $H_{\phi\varepsilon}$ time-dependent functions are then fitted by sinusoidal fonctions at frequency f_{SAW} in order to extract the field-dependence of their amplitudes f_θ, g_ϕ, $h_{\phi\varepsilon}$, respectively. We have $f_\theta = K\delta\theta_0(H)$ and $g_\phi = 2V\delta\phi_0(H)\,|\cos 2\phi_0(H)|$ where $\delta\theta_0$ and $\delta\phi_0$ are the amplitudes of the oscillating $\delta\theta(t)$ and $\delta\phi(t)$, respectively.

In Fig. 3(c) we plot the amplitudes f_θ, g_ϕ, $h_{\phi\varepsilon}$ as a function of the applied field. The amplitude of the PMOKE signal f_θ (black curve) increases progressively to reach a maximum at 22.5 mT and then drops to zero. The MLD component g_ϕ (red curve) shows a different behavior with two maxima and a zero at $\mu_0 H$=16 mT. The $h_{\phi\varepsilon}$ component reflecting a combination of PE and MLD (green curve) has a broad maximum and a clear 40 µrad offset owing to the field-independent elasto-optic effect.

To demonstrate that the physics of the magneto-elastic coupling is responsible for the experimental observations, the magnetization dynamics is modelled in the framework of the Landau-Lifshitz-Gilbert equation including the driving torque generated by the SAW[20]. When the SAW is travelling along [1-10] the torque is mainly driven by the ε_{xx} strain component[16]. We use the sample magnetic parameters (magnetization and magnetic anisotropy) obtained from vibrating sample magnetometer and cavity-FMR experiments. The calculated amplitudes[35] of the magneto-optical signals f_θ and g_ϕ (Fig. 3(d), black and red curves, respectively) show a peak around 25 mT, corresponding to the resonance condition of equal precession and SAW frequencies at f_{SAW} = 301 MHz. The g_ϕ amplitude (red curve) goes to zero at a field such that the static magnetization is at 45° of the easy axis ($\cos 2\phi_0 = 0$). The baseline for $h_{\phi\varepsilon}$ is given by the PE effect that does not depend on the magnetic field. As seen from the comparison of Fig. 3(c) and (d) a good quantitative agreement between experimental and calculated f_θ, g_ϕ, $h_{\phi\varepsilon}$ curves is obtained.

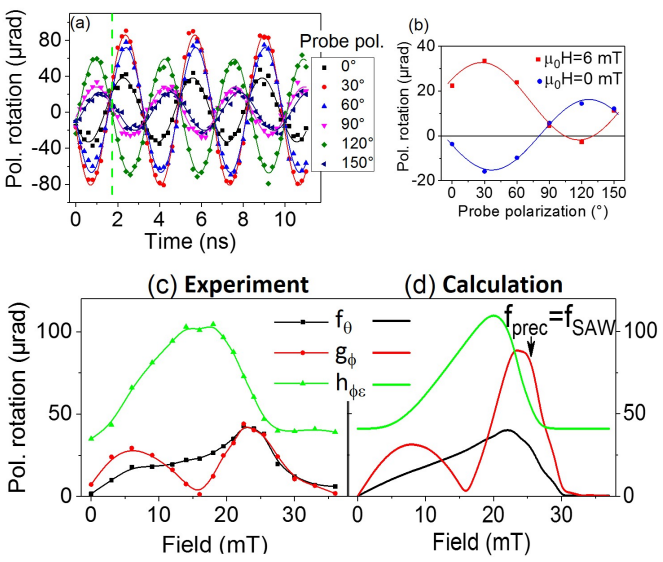

FIG. 3. Polarization and field dependence of the magnetization and strain dynamics for f_{SAW} = 301 MHz at T= 60 K. (a) TRPR signal for six polarization orientations as a function of the optical delay for $\mu_0 H$= 6 mT. (b) TRPR at fixed time delay (cross section of Fig. 3(a), green dashed line) versus probe polarization for two field values. (c) Field variation of the three components f_θ, g_ϕ, $h_{\phi\varepsilon}$ related to polar Kerr effect (β-independent), MLD (cos2β term) and mixed PE/MLD (sin2β term), respectively, at f_{SAW}=301 MHz. (d) Calculated amplitudes of f_θ, g_ϕ, $h_{\phi\varepsilon}$; the parameters are K=18 mrad, V=0.8 mrad, P_E=0.77 rad with $\varepsilon_{xx} = 5.3\,10^{-5}$. The Gaussian distribution on the in-plane anisotropy constant has a standard deviation equal to 12 % of its mean value.

To account for the amplitude and width of f_θ, g_ϕ, $h_{\phi\varepsilon}$ we had to introduce a dispersion of the uniaxial in-plane magnetic anisotropy constant that is known to be crucial for SAW-induced magnetization dynamics[16]. These results show that we are able to disentangle the different contributions in the optical polarization signal and to accurately extract the dynamical magnetic contribution. They provide the first direct, time-domain detection of magneto-acoustic resonance induced by electrically generated *propagating* SAWs. Note that the resonant coupling of optically generated *stationary* SAWs with magnetization had been previously evidenced by Faraday effect in nickel[5,10,13]. In our system, the presence of Kerr and Voigt effects moreover gives access to both the in-plane and out-of-plane dynamical magnetization components.

In order to compare the sensitivity of the magneto-optical signal detection and the SAW amplitude detection after propagation along the layer, we show in Fig. 4 the PMOKE component f_θ (out-of-plane magnetization dynamics) and the variation of the electrically detected SAW amplitude (through the receiving IDT) as a function of the applied magnetic field for the four SAW frequencies. The PMOKE data (top panel of Fig. 4) were normalized by the measured PE level (field-independent

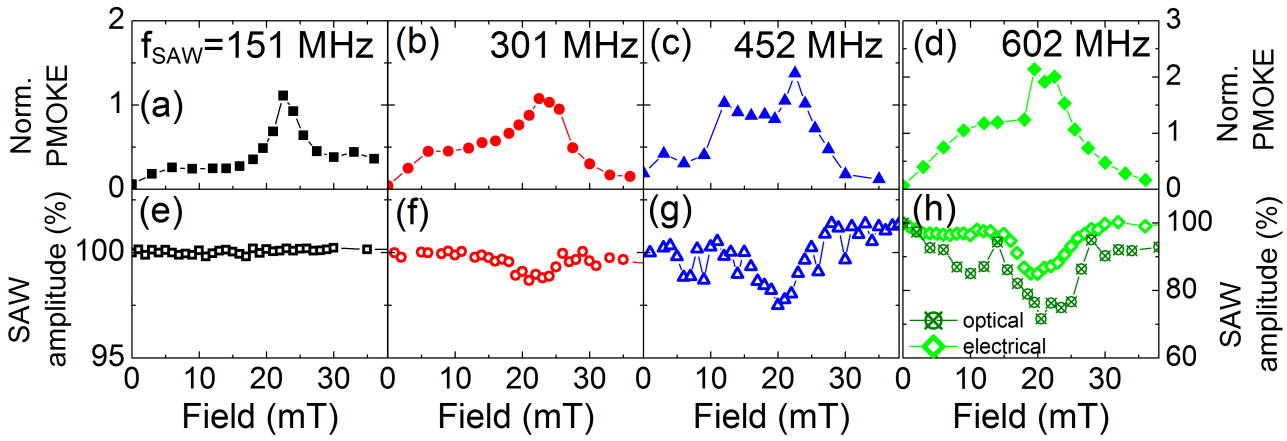

FIG. 4. Top panels: Field dependence of the PMOKE signal (out-of-plane magnetization dynamics) normalized by the field-independent photo-elastic signal for four SAW frequencies at T=60 K. Bottom panels: variation of the SAW amplitude with the magnetic field measured by acoustic-to-electrical conversion at the receiving IDT and in (h) normalized PE signal detected on GaAs in between the GaMnAs mesa and the receiving IDT (see crossed-circle symbol in the schematics of Fig. 2), with a polarization angle β=45 deg. The amplitudes of excited SAW strain components are estimated as $\varepsilon_{xx} = 5.3 \times 10^{-5}$ and $\varepsilon_{zz} = 1.8 \times 10^{-5}$ at f_{SAW}=301 MHz (they are slightly different at other frequencies but low enough to stay in the linear regime).

baseline of $h_{\phi\varepsilon}$) in order to correct for slightly different SAW amplitudes. For each frequency we observe a clear and strong peak of the PMOKE curve at the resonance field (which has close values for the four frequencies because of the steep variation of the FMR frequency with the field[16]). The electrically detected SAW amplitude (bottom panel of Fig. 4) is a rather noisy signal at 151, 301 and 452 MHz, with a much smaller dynamical range. At f_{SAW} = 301, 452, and 602 MHz, it shows a dip at the same field as the peak of the corresponding PMOKE signal. The dip is more pronounced at the higher frequency of 602 MHz as expected from the increase of the absorbed SAW power with the SAW frequency[1,16]. The dip is however not detectable at f_{SAW} = 151 MHz whereas the PMOKE peak is clearly detected. We also plot in Fig. 4(h) the amplitude of the photo-elastic signal detected on GaAs, in between the GaMnAs mesa and the receiving IDT (crossed-circle symbol in the scheme of Fig. 2), normalized by its low-field value. The data was taken for an incoming beam polarisation of 45 deg, which maximizes the strain-induced birefringence. Its field-dependence is similar to that of the electrical signal (Fig. 4(h)) in shape and amplitude. These results show the much larger dynamical range and sensitivity of the magneto-optical SAW-FMR signal, because it is detected on a zero background, with respect to electrical or optical signal of the SAW amplitude variation, detected on a non-zero background.

IV. CONCLUSION

We have developed a sensitive time-domain optical technique to investigate the magneto-elastic coupling between piezo-electrically generated travelling SAWs and magnetization in ferromagnetic layers at variable temperature. The time-resolved magnetization precession was clearly proved to originate from the magneto-elastic coupling with the SAW and shows a resonant behavior at equal SAW and precession frequencies. Compared to the detection of the SAW attenuation, the magneto-optical time-resolved SAW-FMR signal is more sensitive and provides a better signal-to-noise ratio. The detection threshold of the time-resolved signal is mainly governed by the convolution of the SAW wavelength and the laser spot size w. As such, magnetization precession could still be observed at f_{SAW}=900 MHz, for which for $\lambda_{SAW} \sim 3w$. Working at higher SAW frequencies (above 1 GHz) will require a tighter focusing of the laser spot, either by working at higher photon energy (keeping a decent Kerr signal) and/or by increasing the numerical aperture of the focusing objective (keeping a good linear polarization). More generally, we believe that this approach, combining high space/time sensitivity and access to the two components of magnetization will find a wider use in any experiment requiring the synchronization of a radio-frequency electrical stimulus with the ultra-fast optical detection of the magnetic effects it induces, and should benefit broadly the magnetization dynamics community. Applied to magneto-strictive materials, this technique opens the way for a deeper insight into the magnon-phonon coupling and the exploration of the nonlinear regime of acoustic-wave induced magnetization dynamics. Since electrically generated SAWs are a well-mastered technology in microelectronics, SAW-induced magnetization control could be readily implemented in logic or memory devices, with the unprecedented possibility to use wave physics tools such as focusing, diffrac-

tion, and wave-guiding to address a magnetic bit.

ACKNOWLEDGMENTS

This work has been supported by the French Agence Nationale de la Recherche (ANR13-JS04-0001-01). The authors also acknowledge D. Hrabovsky (MPBT-Physical Properties Low Temperature facility of Sorbonne Université), H. J. von Bardeleben (INSP) for magnetometry measurements, and C. Testelin (INSP) for providing scientific equipment.

[1] Dreher, L. *et al.* Surface acoustic wave driven ferromagnetic resonance in nickel thin films: Theory and experiment. *Phys. Rev. B* **86**, 134415 (2012).

[2] Bombeck, M. *et al.* Excitation of spin waves in ferromagnetic (Ga,Mn)As layers by picosecond strain pulses. *Phys. Rev. B* **85**, 195324 (2012).

[3] Li, W., Buford, B., Jander, A. & Dhagat, P. Acoustically assisted magnetic recording: A new paradigm in magnetic data Storage. *IEEE Trans. Mag.* **50**, 37–40 (2014).

[4] Thevenard, L. *et al.* Surface acoustic wave-driven ferromagnetic resonance in (Ga,Mn)(As,P) epilayers. *Phys. Rev. B* **90**, 094401 (2014).

[5] Yahagi, Y., Harteneck, B., Cabrini, S. & Schmidt, H. Controlling nanomagnet magnetization dynamics via magnetoelastic coupling. *Phys. Rev. B* **90**, 140405 (2014).

[6] Shen, K. & Bauer, G. E. Laser-Induced Spatiotemporal Dynamics of Magnetic Films. *Phys. Rev. Lett.* **115**, 197201 (2015).

[7] Davis, S., Borchers, J. A., Maranville, B. B. & Adenwalla, S. Fast strain wave induced magnetization changes in long cobalt bars: Domain motion versus coherent rotation. *J. Appl. Phys.* **117**, 063904 (2015).

[8] Gowtham, P. G., Moriyama, T., Ralph, D. C. & Buhrman, R. A. Traveling surface spin-wave resonance spectroscopy using surface acoustic waves. *J. Appl. Phys.* **118**, 233910 (2015).

[9] Chowdhury, P., Dhagat, P. & Jander, A. Parametric Amplification of Spin Waves Using Acoustic Waves. *IEEE Trans. Mag.* **51**, 1300904 (2015).

[10] Janušonis, J., Chang, C. L., van Loosdrecht, P. H. M. & Tobey, R. I. Frequency tunable surface magneto-elastic waves. *Appl. Phys.Lett.* **106**, 181601 (2015).

[11] Thevenard, L. *et al.* Strong reduction of the coercivity by a surface acoustic wave in an out-of-plane magnetized epilayer. *Phys. Rev. B* **93**, 140405 (2016).

[12] Thevenard, L. *et al.* Precessional magnetization switching by a surface acoustic wave. *Phys. Rev. B* **93**, 134430 (2016).

[13] Chang, C. L. *et al.* Parametric frequency mixing in a magnetoelastically driven linear ferromagnetic resonance oscillator. *Phys. Rev. B* **95**, 060409 (2017).

[14] Hashimoto, Y. *et al.* All-optical observation and reconstruction of spin wave dispersion. *Nat. Commun.* **8**, 15859 (2017).

[15] Kim, J.-W. & Bigot, J.-Y. Magnetization precession induced by picosecond acoustic pulses in a freestanding film acting as an acoustic cavity. *Phys. Rev. B* **95**, 144422 (2017).

[16] Kuszewski, P. *et al.* Resonant magneto-acoustic switching: influence of Rayleigh wave frequency and wavevector. *J. Phys.: Cond. Mat.* **30**, 244003 (2018).

[17] Shihab, S., Thevenard, L., Lemaître, A. & Gourdon, C. Counter-rotating standing spin waves: A magneto-optical illusion. *Phys. Rev. B* **95**, 144411 (2017).

[18] Foerster, M. *et al.* Direct imaging of delayed magneto-dynamic modes induced by surface acoustic waves. *Nat. Comm.* **8**, 407 (2017).

[19] Linnik, T. L. *et al.* Theory of magnetization precession induced by a picosecond strain pulse in ferromagnetic semiconductor (Ga,Mn)As. *Phys. Rev. B* **84**, 214432 (2011).

[20] Thevenard, L. *et al.* Irreversible magnetization switching using surface acoustic waves. *Phys. Rev. B* **87**, 144402 (2013).

[21] Yeo, L. Y. & Friend, J. R. Surface Acoustic Wave Microfluidics. *Annu. Rev. Fluid Mech.* **46**, 379 (2014).

[22] Mamishev, A. V., Sundara-Rajan, K., Yang, F., Du, Y. & Zahn, M. Interdigital sensors and transducers. *Proc. IEEE* **92**, 808 (2004).

[23] Poole, T. & Nash, G. R. Acoustoelectric Current in Graphene Nanoribbons. *Sci. Rep.* **7**, 1767 (2017).

[24] De Lima, M. M. & Santos, P. V. Modulation of photonic structures by surface acoustic waves. *Rep. Prog. Phys.* **68**, 1639 (2005).

[25] Neubrand, A. & Hess, P. Laser generation and detection of surface acoustic waves: Elastic properties of surface layers. *J. Appl. Phys.* **71**, 227 (1992).

[26] Royer, D. & Dieulesaint, E. *Elastic Waves in Solids II. Generation, Acousto-optic Interaction, Application* (Springer-Verlag, Berlin, 2000).

[27] Schülein, F. J. *et al.* Fourier synthesis of radiofrequency nanomechanical pulses with different shapes. *Nat. Nanotechnol.* **10**, 512 (2015).

[28] Holländer, R. B., Müller, C., Lohmann, M., Mozooni, B. & McCord, J. Component selection in time-resolved magneto-optical wide-field imaging for the investigation of magnetic microstructures. *J. Magn. Magn. Mater.* **432**, 283 (2017).

[29] Weiß, M. *et al.* Multiharmonic Frequency-Chirped Transducers for Surface-Acoustic-Wave Optomechanics. *Phys. Rev. Appl.* **9**, 014004 (2018).

[30] Maichen, W. *Digital timing measurements: from scopes and probes to timing and jitter* (Springer Science & Business Media, 2006).

[31] Němec, P. *et al.* Experimental observation of the optical spin transfer torque. *Nat. Phys.* **8**, 411 (2012).

[32] Royer, D. & Dieulesaint, E. *Elastic Waves in Solid I: Free and Guided Propagation* (Springer-Verlag, Berlin Heidel-

berg, 2000).

[33] Saito, T., Matsuda, O., Tomoda, M. & Wright, O. B. Imaging gigahertz surface acoustic waves through the photoelastic effect. *J. Opt. Soc. Am. B* **27**, 2632 (2010).

[34] Santos, P. V. Acoustic field mapping on GaAs using microscopic reflectance and reflectance anisotropy. *Appl. Phys. Lett.* **74**, 4002 (1999).

[35] Because we are only considering the uniform FMR mode, it is unecessary to take into account the absorption and optical phase shift of the light in the layer, as in Ref. 17..